PROCEEDINGS A

rspa.royalsocietypublishing.org

Review

Check for updates

Article submitted to journal

Subject Areas:
applied mathematics, analysis, computational mathematics

Keywords:
van der Pauw method, prime function, Fay trisecant identity

Author for correspondence:
Hiroyuki Miyoshi
e-mail:
hiroyuki.miyoshi17@imperial.ac.uk

Fay meets van der Pauw: the trisecant identity and the resistivity of holey samples

Hiroyuki Miyoshi[1], Darren G. Crowdy[1] and Rhodri Nelson[2]

[1]Department of Mathematics, Imperial College London, 180 Queen's Gate, London SW7 2AZ, UK
[2]Department of Earth Science and Engineering, Imperial College London, 180 Queen's Gate, London SW7 2AZ, UK

The van der Pauw method is commonly used in the applied sciences to find the resistivity of a simply connected, two-dimensional conducting laminate. Given the usefulness of this "4-point probe" method there has been much recent interest in trying to extend it to holey, that is, multiply connected, samples. This paper introduces two new mathematical tools to this area of investigation – the prime function on the Schottky double of a planar domain and the Fay trisecant identity – and uses them to show how the van der Pauw method can be extended to find the resistivity of a sample with a hole. We show that an integrated form of the Fay trisecant identity provides valuable information concerning the appearance of "envelopes" observed in the case of holey samples by previous authors. We find explicit formulas for these envelopes, as well as an approximate formula relating two pairs of resistance measurements to the sample resistivity that is expected to be valid when the hole is sufficiently small and not too close to the outer boundary. We describe how these new mathematical tools have enabled us to prove certain conjectures recently made in the engineering literature.

1. Introduction

Sheet resistances and Hall coefficients are key parameters for the performance of semiconductors and conducting materials and methods for measuring these important material properties have been extensively studied [1].

THE ROYAL SOCIETY PUBLISHING

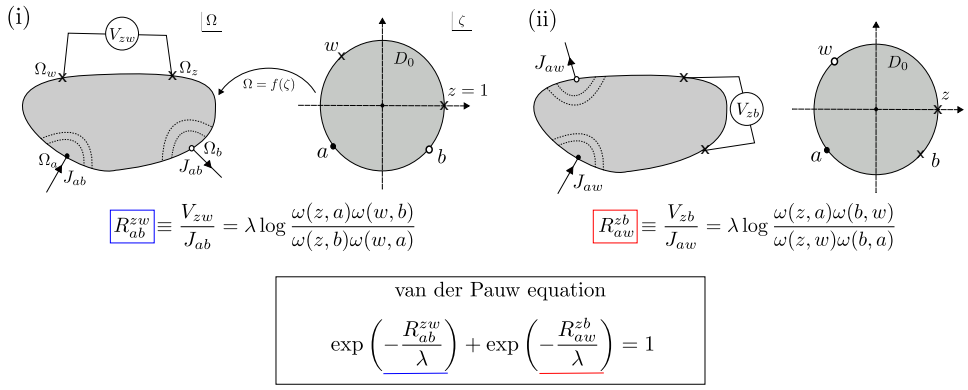

Figure 1. The original van der Pauw set-up. The first measurement is the voltage difference between z and w with a source of current a and a sink of current b. The second measurement is the difference between z and b with a source a and a sink w. These resistances satisfy the van der Pauw equation (1.1) which can be solved for λ.

One of the most prevalent and successful measurement techniques is the four-point probe method; a recent centenary review of this method [2] provides a comprehensive survey of the vast literature on such methods. While the basic idea of a four-point measurement dates back to early work by Wenner [2] who was trying to measure the resistivity of the Earth, van der Pauw [3,4] pointed out that the basic idea of the four-point method works for determining the resistivity of uniform two-dimensional samples of *any* shape provided the contacts are placed at the edges of the sample. Samples must have a flat shape of uniform thickness, be isotropic of uniform resistivity, and be simply connected (no holes). Extensions of the method to contacts of finite width have been made [5]. These powerful four-point methods have perennial importance and have been applied to modern materials such as graphene [6].

Figure 1 shows a setup for the original van der Pauw measurement: the four electrical contacts $(\Omega_a, \Omega_b, \Omega_z, \Omega_w)$ are placed on the perimeter of a test sample. If Ω_a and Ω_b are a source and sink of current J_{ab} respectively, then the potential difference V_{zw} between points Ω_z and Ω_w can be measured while this current is flowing. The resistance $R^{zw}_{ab} = V_{zw}/J_{ab}$ is then a measured quantity; a second resistance R^{zb}_{aw} can be measured in exactly the same way. Van der Pauw [4] showed that for any arrangement of four electrical contacts, and given these two resistance measurements R^{zw}_{ab} and R^{zb}_{aw}, the resistivity λ can be found by solving the nonlinear equation:

$$\exp\left(-\frac{R^{zw}_{ab}}{\lambda}\right) + \exp\left(-\frac{R^{zb}_{aw}}{\lambda}\right) = 1. \tag{1.1}$$

We will refer to this as the classical *van der Pauw equation* and it provides the basis for the van der Pauw method. Because this method needs only two resistance measurements, and works for samples of arbitrary shape, the method is widely applied for measuring the resistivity of superconductors or Hall coefficients of materials in laboratory experiments [3,7]. An efficient numerical method to determine λ is discussed in [8].

While applied scientists might be familiar with the van der Pauw equation (1.1) mathematicians are perhaps more familiar with a similar-looking *cross-ratio identity* given by

$$p_0(z,w;b,a) + p_0(z,b;w,a) = 1, \tag{1.2}$$

where the classical cross-ratio is defined by

$$p_0(z,w;a,b) \equiv \frac{\omega(z,a)\omega(w,b)}{\omega(z,b)\omega(w,a)}, \tag{1.3}$$

and where, in a step usually not carried out, we introduce the *prime function* [9] as the simple monomial function of two complex variables, ζ and c say, defined by

$$\omega(\zeta, c) = \zeta - c. \tag{1.4}$$

Establishing the identity (1.2) is a simple exercise. In complex analysis the cross-ratio [9,10] is most commonly encountered in a geometrical context as the Möbius mapping that provides a conformal mapping, as a function of the variable z say, between 3 arbitrary complex points (a, w, b) in the complex z plane and the canonical choice of points $(0, 1, \infty)$.

Concerning the function (1.4), it is so simple in this case that it is rarely given the designation "prime function". However, the monograph [9] makes the case that recognizing it as the simplest instance of a more general notion of a *prime function* is important for generalizing many known results for simply connected planar geometries to multiply connected cases. The van der Pauw problem of interest here is no exception. It will be shown later that the natural way to extend the classical van der Pauw method to multiply connected geometries is to treat the problem using the prime function – more specifically, the multiply connected generalization of (1.4) – and to make use of some important identities satisfied by that function.

There is a connection between (1.1) and (1.2). It can be elucidated by considering the complex potential $H_0(\Omega)$ of the complex variable $\Omega = x + \mathrm{i}y$, where (x, y) denotes Cartesian coordinates in the physical plane, whose real part is the harmonic voltage potential $V(x, y)$ in the sample:

$$H_0(\Omega) = V(x, y) + \mathrm{i}\chi(x, y), \tag{1.5}$$

where we have introduced $\chi(x, y)$, the harmonic conjugate of $V(x, y)$. The voltage $V(x, y)$ is harmonic in the sample and its normal derivative vanishes on the sample boundary; equivalently, by the Cauchy-Riemann equations, its harmonic conjugate $\chi(x, y)$ is constant on the boundary. Let σ be the sought-after resistivity of the sample. Its thickness, measured beforehand, is denoted by d.

By the Riemann mapping theorem, we can introduce a conformal mapping $\Omega = f(\zeta)$ between the unit disc in a complex parametric ζ plane and the sample in the physical Ω plane. By the conformal invariance of the boundary value problem for $V(x, y)$ [10], the complex potential $h_0(\zeta) \equiv H_0(\Omega)$ for the voltage distribution caused by a current source at Ω_a and a compensating sink at Ω_b is then given, as a function of ζ, by

$$h_0(\zeta) = \frac{\sigma J_{ab}}{\pi d} \log\left(\frac{\omega(\zeta, a)}{\omega(\zeta, b)}\right), \tag{1.6}$$

where,

$$\Omega_a = f(a), \qquad \Omega_b = f(b). \tag{1.7}$$

The reader will notice that the prime function (1.4) appears in (1.6). The potential difference V_{zw} is therefore given by

$$V_{zw} \equiv \mathrm{Re}[h_0(z)] - \mathrm{Re}[h_0(w)] = \lambda J_{ab} \log\left|\frac{\omega(z, a)\omega(w, b)}{\omega(z, b)\omega(w, a)}\right| = \lambda J_{ab} \log|p_0(z, w; a, b)|, \tag{1.8}$$

where $\lambda \equiv \sigma/(\pi d)$. It follows that

$$R_{ab}^{zw} = \frac{V_{zw}}{J_{ab}} = \lambda \log p_0(z, w; a, b), \tag{1.9}$$

where we have removed the modulus symbols because the cross-ratio is real and positive when all (z, w, a, b) are on the unit circle in the ζ plane, and $0 \le \arg[z] < \arg[w] < \arg[a] < \arg[b] < 2\pi$. On combining (1.9) with (1.2), we arrive at the van der Pauw equation (1.1).

In recent years, the van der Pauw method for samples with a single hole, or even several holes, has been extensively studied [11–20]. It has been reported that the van der Pauw equation (1.1) is inaccurate for samples with several holes [21]. This is to be expected since this formula takes no account of the presence of any holes. Indeed, quite what form the appropriate generalization of

the van der Pauw method should take is not currently clear from the extant literature. The present paper aims to shed light on this matter.

A sample with a single isolated hole whose boundary comprises more than a single point is the natural first case to study and has been considered by [11,16]. Any 2D sample with a single hole is doubly connected and can be transplanted conformally into an annulus [9] where the radius of the inner circle of the annulus depends on the shape of sample [22]. By conducting both numerical and laboratory experiments Szymański et al. [11] showed that the van der Pauw equation (1.1) does not hold for a sample with a hole but conjectured that the data instead satisfies the inequality

$$\exp\left(-\frac{R_{ab}^{zw}}{\lambda}\right)+\exp\left(-\frac{R_{aw}^{zb}}{\lambda}\right)\leq 1. \tag{1.10}$$

This inequality has been conjectured in series of papers [12,13] but, to the best of the authors' knowledge, no rigorous proof has yet been given. One objective of this paper to show how the inequality (1.10) can be confirmed mathematically.

For holey samples Szymański et al. proposed some modifications to the van der Pauw setting [12,16]. Firstly, they proposed a six-point method, which uses six electrical contacts on the perimeter of a sample with a hole, and measures nine pairs of resistances [16]. Because the nine resistances can be expressed explicitly in terms of the coordinates of six electrical contacts on the perimeter of a unit circle, they obtained a well-conditioned equation for the unknown sample resistivity. The method was also validated by some laboratory experiments. Arguably a drawback is that the method requires the measurement of nine resistances to solve seven nonlinear equations.

Szymański et al. [12] also find that the pair of measured resistance $(R_{ab}^{zw}, R_{aw}^{zb})$ satisfies another inequality which they dubbed a "lower envelope" – a phrase we also adopt – and they proposed a method to measure the resistivity based on the existence of this envelope. By conjecturing that the shape of the lower envelope depends only on a Riemann modulus ρ, they applied a standard fitting technique for pairs of measurements $(R_{ab}^{zw}, R_{aw}^{zb})$ lying on this envelope and consequently were able to determine the sample resistivity. They did not, however, find a mathematical expression for this lower envelope. This is one of the new contributions of the present paper which we now describe.

Figure 2 shows the results of the same numerical experiment conducted in [12]. It shows the data from 40,000 pairs (X, Y), where the more convenient designations

$$X\equiv\exp(-R_{ab}^{zw}/\lambda),\qquad Y\equiv\exp(-R_{aw}^{zb}/\lambda) \tag{1.11}$$

are introduced. In Figure 2 three different samples are used, corresponding to three different values of ρ. The contact points z, w, a, and b are chosen at random but always such that they retain the ordering $0=\arg[z]<\arg[w]<\arg[a]<\arg[b]<2\pi$. The data is found to fall in the gray-shaded regions in Figure 2. If there is no hole, which means $\rho=0$, the pair satisfies $X+Y=1$ as must be true since that data is known to satisfy the original van der Pauw equation (1.1). However, if $\rho>0$, this is no longer true and the data (X, Y) "fills in" a crescent-shaped domain shown shaded in Figure 2. Szymański et al. conjecture that the data (X, Y) always lies in such a domain bounded by the upper envelope $X+Y\leq 1$ and some lower envelope, dependent purely on ρ. Those authors do not, however, give a definite equation for the curve described by this envelope. The same authors also conjecture, again without a rigorous mathematical proof, that the lower envelope might correspond to the pair of (X_θ, Y_θ), where (X_θ, Y_θ) are measurements with the four electrical contacts having the "symmetry" shown on the right of Figure 3; for brevity, we will refer to these as "symmetric resistance measurements". The angle θ is defined as $\theta\equiv\arg[w/z]=\arg[b/a]$; for such contact points the sector formed by the pair (a, b) subtends the same angle θ at the origin as that formed by the pair (z, w). Based on these conjectures, Szymański et al. [12] propose a method to determine λ by measuring some pairs of resistances which lie on the lower envelope. If these conjectures hold then the form of the upper and lower envelopes can be expressed mathematically

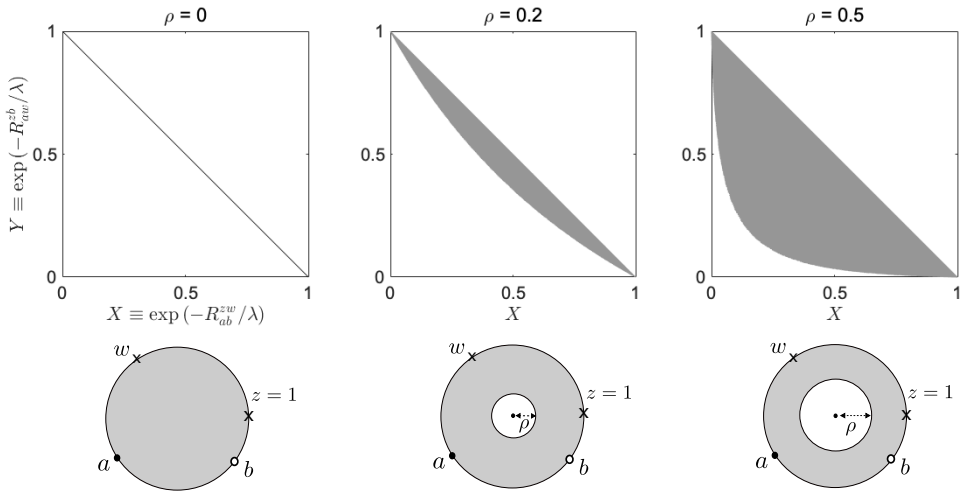

Figure 2. Evidence for the two "envelopes". Numerical experiments for pairs (X, Y) where $X \equiv \exp(-R^{zw}_{ab}/\lambda)$ and $Y \equiv \exp(-R^{zb}_{aw}/\lambda)$ following [12]. The point $z = 1$ is fixed, but (a, b, w) are picked at random with the ordering $\arg[z] < \arg[w] < \arg[a] < \arg[b] < 2\pi$. When $\rho = 0$, all pairs (X, Y) are on the line $X + Y = 1$ which is (1.1). However, when $\rho > 0$, all points (X, Y) lie in the gray-shaded region bounded by $X + Y = 1$ and a "lower envelope" which is curved. As shown in the center and right, the size of the gray-shaded area increases with ρ.

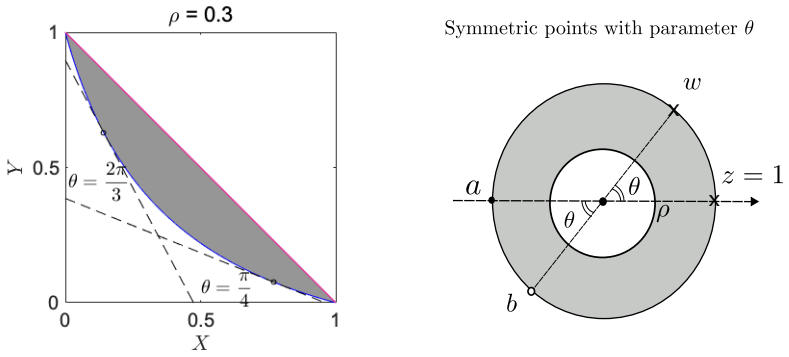

Figure 3. The upper envelope (red line) and the lower envelope (blue line). The lower envelope, parametrized by the variable θ, is defined by its set of tangents as in (1.12): any point in the gray region, which is where all measurement pairs lie, is above the tangent line for each point on the lower envelope. The right-most figure gives a geometrical interpretation of θ and shows what we mean by "symmetric resistance measurements": the sector formed by the pair (a, b) subtends the same angle θ at the origin as that formed by the pair (z, w).

as

$$X + Y \le 1, \qquad Y - Y_\theta \ge \frac{\partial Y_\theta/\partial\theta}{\partial X_\theta/\partial\theta}(X - X_\theta), \qquad 0 < \theta < \pi, \tag{1.12}$$

where θ parametrizes the lower envelope which is defined by its set of tangents. Two examples of such tangents (1.12) are shown on the left of Figure 3. These inequalities have been put forward in several papers [11–14] but without mathematical substantiation.

This paper aims to understand the envelope structure mathematically. This is done by introducing, for the first time, two important tools into this area of investigation: (i) use of the

prime function [9] associated with the concentric annulus $\rho < |\zeta| < 1$ that generalizes the simple monomial prime function (1.4) relevant when the sample if free of holes; (ii) use of the Fay trisecant identity [9,23,24] satisfied by this new prime function to gain insights into the two envelopes associated with the two resistance measurements (1.11).

With these tools we are able to establish three main new results.

First, the following explicit formula for the lower envelope is derived:

$$\int_0^{2\pi} \log\left(\exp\left(-\frac{R_X^\theta}{\lambda}\right) + \frac{P(-\rho e^{\mathrm{i}\phi})^2}{P(+\rho e^{\mathrm{i}\phi})^2}\exp\left(-\frac{R_Y^\theta}{\lambda}\right)\right) d\phi = 0, \tag{1.13}$$

where R_X^θ and R_Y^θ are resistance measurements corresponding to contact points (a, b, z, w) with the symmetry depicted in Figure 3 and parametrized by the angle θ shown there; for a fixed ρ and λ, formula (1.13) therefore defines a curve as θ varies between 0 and π and this is precisely the lower envelope. The function $P(\zeta)$, defined in (2.4), is essentially the prime function of the concentric annulus.

Equation (1.13) includes two unknown parameters ρ and λ. By measuring two pairs of resistances $(R_X^{\theta_j}, R_Y^{\theta_j})$, $j = 1,\ 2$, for two sets of contact points with different angles θ_1 and θ_2 in the symmetric arrangement shown in Figure 3, λ can be determined by solving two simultaneous equations of the form (1.13) for ρ and λ. This procedure is elucidated in more detail in §5.

It should be pointed out that the new expression (1.13) explicitly confirms the conjecture of Szymański et al. [12] that the lower envelope depends only on the value of the conformal modulus ρ. Indeed, using the new mathematical tools introduced herein, we have been able to prove mathematically several conjectures made by Szymański et al. [12] including the two inequalities (1.12) defining the upper and lower envelopes. Full technical details of those proofs will be given elsewhere [25] but the main ideas will be outlined here too. Formula (1.13) emerges as a by-product of our approach.

Second, we produce an *approximate* formula directly relating two pairs of symmetric resistance measurements $(R_X^{\theta_j}, R_Y^{\theta_j})$, $j = 1,\ 2$, and λ, under the assumption that ρ is sufficiently small that terms of $\mathcal{O}(\rho^4)$ can be safely ignored. That new formula is

$$\begin{aligned}\exp\left(\frac{R_X^{\theta_1} - R_Y^{\theta_1}}{\lambda}\right) + \exp\left(\frac{R_Y^{\theta_1} - R_X^{\theta_1}}{\lambda}\right) - \exp\left(\frac{R_X^{\theta_1} + R_Y^{\theta_1}}{\lambda}\right) = \\ \exp\left(\frac{R_X^{\theta_2} - R_Y^{\theta_2}}{\lambda}\right) + \exp\left(\frac{R_Y^{\theta_2} - R_X^{\theta_2}}{\lambda}\right) - \exp\left(\frac{R_X^{\theta_2} + R_Y^{\theta_2}}{\lambda}\right).\end{aligned} \tag{1.14}$$

The significance of equation (1.14) is that it more closely resembles the classical van der Pauw equation (1.1) since it depends only on λ and the resistance measurements although, in this case, there are 4 such measurements involved not just 2. The important point is that dependence on ρ has disappeared in (1.14). An approximation for λ can be calculated by solving the single equation (1.14) provided that the two pairs of resistance measurements $(R_X^{\theta_j}, R_Y^{\theta_j})$, $j = 1,\ 2$ corresponding to "symmetric" contact points are available.

Third, we are also able to justify mathematically a practical procedure for obtaining such "symmetric" resistance measurements for a general non-symmetric sample as proposed by Szymański et al. [12]. Those authors gave evidence that their practical construction produces such data, but did not appear to give any mathematical justification as to why the method works.

The paper is structured as follows. In §2 the prime function for the annulus is introduced and, in §3, the Fay trisecant identity satisfied by this particular prime function is presented. Section 4 shows how these mathematical tools can be used to understand the structure of the envelopes associated with a holey sample. This involves analysis of an integrated form of the Fay trisecant identity. In §5 we propose how to use the new expressions for the lower envelope curve in a generalized van der Pauw setting and carry out some numerical tests to validate the scheme. The paper closes with a discussion of new perspectives opened up by our analysis for samples with more than one hole.

2. The prime function for the annulus $\rho < |\zeta| < 1$

Let D denote a bounded sample with an isolated hole. Let ∂D_0 be the outer boundary of the sample and ∂D_1 the boundary of the hole. Similar to the original van der Pauw method, we assume that the sample thickness is d. We assume that the hole in the sample carries no net charge.

We also suppose that 4 point contacts $(\Omega_a, \Omega_b, \Omega_z, \Omega_w)$, of infinitesimal width, are placed on ∂D_0. It is known, by an extension of the Riemann mapping theorem [9], that any such domain is conformally equivalent to a concentric annulus $\rho < |\zeta| < 1$ with circular boundaries C_0 and C_1 and $0 \leq \rho < 1$. The circle C_0 is the unit circle; C_1 is the circle $|\zeta| = \rho$. In other words, there exists an analytic function

$$\Omega = f(\zeta) \tag{2.1}$$

that transplants the annulus $\rho < |\zeta| < 1$ to the domain D with C_0 being transplanted to ∂D_0 and C_1 to ∂D_1.

Let the required complex potential, as a function of $\Omega = x + \mathrm{i}y$ be

$$H(\Omega) = V(x, y) + \mathrm{i}\chi(x, y). \tag{2.2}$$

We can still exploit the conformal invariance for the problem of determining the potential $V(x, y)$ in this doubly connected domain. Crowdy [9,26] has shown that the complex potentials for any source/sink driven harmonic field in a multiply connected domain can be written down explicitly in terms of the prime function associated with that domain. It is important to emphasize that this fact holds for domains of any finite connectivity not just the doubly connected case of interest here.

The prime function $\omega(\zeta, c)$ for the annulus $\rho < |\zeta| < 1$, can be defined explicitly by the formula (see [9]):

$$\omega(\zeta, c) = -\frac{c}{\hat{P}(1)} P(\zeta/c), \tag{2.3}$$

where

$$P(\zeta) \equiv (1 - \zeta)\hat{P}(\zeta), \qquad \hat{P}(\zeta) \equiv \prod_{n=1}^{\infty} (1 - \rho^{2n}\zeta)(1 - \rho^{2n}/\zeta). \tag{2.4}$$

It is easy to show, directly from these definitions, that

$$P(\zeta^{-1}) = -\zeta^{-1} P(\zeta), \qquad P(\rho^2\zeta) = -\zeta^{-1} P(\zeta). \tag{2.5}$$

For notational brevity, we write $P(\zeta)$ even though this function – and hence the prime function for the annulus – *also* depends on the parameter ρ as is clear from (2.4). The reader should bear in mind this additional parametric dependence on ρ. We will also need

$$K(\zeta) \equiv \zeta \frac{\partial}{\partial \zeta} \log P(\zeta). \tag{2.6}$$

This logarithmic derivative of the prime function is a useful function in the general function theory on multiply connected domains [9]. It is easily shown to satisfy the functional relations

$$K(\zeta^{-1}) = 1 - K(\zeta), \qquad K(\rho^2\zeta) = K(\zeta) - 1. \tag{2.7}$$

A detailed account of the theory of this prime function in the concentric annulus can be found in Chapter 5 of [9].

Following [9,26] the complex potential $h(\zeta) \equiv H(f(\zeta))$ is given by

$$h(\zeta) = \frac{\sigma J_{ab}}{2\pi d} \log\left(\frac{\bar{a}b}{|ab|} \frac{\omega(\zeta, a)\omega(\zeta, \bar{a}^{-1})}{\omega(\zeta, b)\omega(\zeta, \bar{b}^{-1})}\right) = \lambda J_{ab} \log\left(\frac{a}{b} \frac{P(\zeta/a)}{P(\zeta/b)}\right), \tag{2.8}$$

where the first equality is derived in [9,26] and follows from the general properties of the prime function, and where we have used (2.3) in the second equality. The relation (2.1) gives the relationship between (a, b, z, w) and $(\Omega_a, \Omega_b, \Omega_z, \Omega_w)$ although it is understood that the mapping

$f(\zeta)$ is now the new mapping from the concentric annulus to the holey sample. Note that, because two electrical contacts a and b are on C_0, $\bar{a} = a^{-1}$ and $\bar{b} = b^{-1}$.

The voltage difference between z and w is given by

$$V_{zw} \equiv \mathrm{Re}[h(z)] - \mathrm{Re}[h(w)] = \lambda J_{ab} \log \frac{P(z/a)P(w/b)}{P(z/b)P(w/a)}. \tag{2.9}$$

It is important to note that because all contacts are located on the same boundary of the annulus, $\mathrm{Im}[h(z)] - \mathrm{Im}[h(w)] = 0$. The measured resistances R_{ab}^{zw} and R_{aw}^{zb} are defined as

$$R_{ab}^{zw} \equiv \frac{V_{zw}}{J_{ab}} = \lambda \log \frac{P(z/a)P(w/b)}{P(z/b)P(w/a)}, \qquad R_{aw}^{zb} \equiv \frac{V_{zb}}{J_{aw}} = \lambda \log \frac{P(z/a)P(b/w)}{P(z/w)P(b/a)}. \tag{2.10}$$

It can be checked that formulas (2.10) are equivalent to those given in [11] in terms of a function $G(\phi)$ related to $P(\zeta)$ – and hence to the prime function (2.3) – by the formula

$$P(e^{\mathrm{i}\phi}) = -2\mathrm{i}e^{\frac{\mathrm{i}\phi}{2}} \hat{P}(\mathrm{i}) G(\phi). \tag{2.11}$$

While (2.11) shows that our new expressions (2.10) coincide with those of [11], there is much significance in having recognized that the resistances can be written in terms of the prime function [9] of the preimage concentric annulus. First, the notion of a prime function extends to a planar domain of any finite connectivity [9] thereby providing a route to generalizing all the ideas in this paper to any higher connected domain (i.e. a sample with more than one hole). Crowdy [26] was the first to show how the complex potentials for source/sink driven harmonic fields in multiply connected domains can be written explicitly. His treatment uses irrotational fluid mechanics as the physical context but, mathematically, the problem is equivalent to the electrical conduction problems of interest here. Second, it is known [9] that prime functions, including those associated with domains of connectivity higher than one, satisfy a so-called Fay trisecant identity which is an analogue of the cross-ratio identity (1.2) on a higher genus Riemann surface [23] and is the topic of the next section.

3. The Fay trisecant identity for the annulus $\rho < |\zeta| < 1$

It is useful to introduce the function

$$p(z, w; a, b) \equiv \frac{\omega(z, a)\omega(w, b)}{\omega(z, b)\omega(w, a)}. \tag{3.1}$$

Although this formula is identical to that defining the cross-ratio (1.2) this quantity is no longer a cross-ratio since the definition of the prime function has changed. On use of (2.3) formula (3.1) can be written in terms of $P(\zeta)$ as

$$p(z, w; a, b) = \frac{P(z/a)P(w/b)}{P(z/b)P(w/a)}. \tag{3.2}$$

From (3.2) and (2.10) we see that

$$\exp(-R_{ab}^{zw}/\lambda) = p(z, w; b, a), \qquad \exp(-R_{aw}^{zb}/\lambda) = p(z, b; w, a). \tag{3.3}$$

The Fay trisecant identity associated with this prime function is

$$\frac{P(kz/w)P(ka/b)}{P(kza/wb)} p(z, w; b, a) + \frac{P(kz/b)P(ka/w)}{P(kza/wb)} p(z, b; w, a) = P(k), \tag{3.4}$$

where k is an arbitrary complex number. This statement (3.4) of the genus-1 Fay trisecant identity expressed purely in terms of the prime function of the concentric annulus has been taken from Exercise 8.9 of Chapter 8 of the monograph [9] which asks the reader to prove it using the properties of so-called loxodromic functions. While (3.4) is a particular form of the more general Fay trisecant identity [23,24] the authors have not found it written in the form (3.4) anywhere else in the literature (besides [9]). The identity (3.4) is stated here without proof since it is easily shown to hold for any choice of k, a, b, z and w on use of the functional relations (2.5).

A key observation is that, on substituting (2.10) into (3.4), we obtain

$$\frac{P(kz/w)P(ka/b)}{P(k)P(kza/wb)}\exp\left(-\frac{R_{ab}^{zw}}{\lambda}\right)+\frac{P(kz/b)P(ka/w)}{P(k)P(kza/wb)}\exp\left(-\frac{R_{aw}^{zb}}{\lambda}\right)=1\,. \tag{3.5}$$

When $\rho\to 0$, so that there is no hole in a sample, it is straightforward to check that

$$\frac{P(kz/w)P(ka/b)}{P(k)P(kza/wb)}=\frac{P(kz/b)P(ka/w)}{P(k)P(kza/wb)}=1 \tag{3.6}$$

because, from (2.4), $P(\zeta)=1-\zeta$ when $\rho=0$. The original van der Pauw equation (1.1) is therefore retrieved from (3.5) in the simply connected (i.e. "no hole") limit. All dependence on the new parameter k disappears in this limit.

The title of this paper is chosen because it appears to be the first to point out that the Fay trisecant identity can be expressed in terms of the two resistances appearing in a typical van der Pauw procedure as evinced in (3.5). Relation (3.5) opens up new perspectives: that it reduces, as $\rho\to 0$, to the original van der Pauw equation (1.1) is tantalizing. It also makes it a natural candidate, at least from the mathematical point of view, to find natural ways to extend the van der Pauw method to holey samples. In contrast to the original van der Pauw equation, the coefficients of $\exp(-R_{ab}^{zw}/\lambda)$ and $\exp(-R_{aw}^{zb}/\lambda)$ in (3.5) now depend not only on the electrical contact locations via the parameters z, w, a, b as well as the conformal modulus ρ, but also on a fifth complex parameter k. For a given ρ it should be emphasized that (3.5) holds for arbitrary choices of a, b, z, w and k even though, for present purposes, it has been assumed that a, b, z and w lie on C_0. The degree of freedom in the choice of k will be exploited in the next section to gain insights into the envelope structure evident in Figure 2.

4. Analysis of the envelopes: the integrated Fay identity

In §1 the existence of two envelopes, an "upper" and a "lower" envelope, were discussed based on the observations of previous authors. These envelopes have the conjectured mathematical definitions given in (1.12). In this section it is shown how the new tools introduced in the previous two sections allow us to prove the conjectured form of these envelopes.

For arbitrary z, w, a, and b on C_0 we can introduce the special choice of angular coordinates θ, θ_1 and θ_3 defined by

$$z=1,\qquad w=\exp(\mathrm{i}(\theta_1+\theta)),\qquad a=\exp(\mathrm{i}(\theta_1+\theta_3)),\qquad b=\exp(\mathrm{i}(\theta+\theta_3)). \tag{4.1}$$

The arbitrary points with the angular coordinates is described in Figure 4. Because $0<\arg[w]<\arg[a]<\arg[b]<2\pi$, the ranges of $\theta_1,\ \theta,\ \theta_3$ are given by

$$-\theta<\theta_1<\theta,\qquad \theta<\theta_3<2\pi-\theta,\qquad 0<\theta<\pi. \tag{4.2}$$

It is important to emphasize that the case of symmetric contact points shown in Figure 3 corresponds to $\theta_1=0$ and $\theta_3=\pi$. The choice (4.1) of angular variables may not seem very intuitive but they have been chosen because they allow us to make progress with the proofs.

The Fay trisecant identity (3.5) can be written

$$A(\theta_1,\theta,\hat{k})X_{\theta_1,\theta_3,\theta}+B(\theta_3,\theta,\hat{k})Y_{\theta_1,\theta_3,\theta}=1, \tag{4.3}$$

where $X_{\theta_1,\theta_3,\theta}\equiv\exp(-R_{ab}^{zw}/\lambda)$, $Y_{\theta_1,\theta_3,\theta}\equiv\exp(-R_{aw}^{zb}/\lambda)$ and the coefficient functions are

$$A(\theta_1,\theta,\hat{k})\equiv\frac{P(kz/w)P(ka/b)}{P(k)P(kza/wb)}=\frac{P(ke^{-\mathrm{i}(\theta+\theta_1)})P(ke^{\mathrm{i}(-\theta+\theta_1)})}{P(k)P(ke^{-2\mathrm{i}\theta})}=\frac{P(\hat{k}e^{-\mathrm{i}\theta_1})P(\hat{k}e^{\mathrm{i}\theta_1})}{P(\hat{k}e^{-\mathrm{i}\theta})P(\hat{k}e^{\mathrm{i}\theta})}, \tag{4.4}$$

$$B(\theta_3,\theta,\hat{k})\equiv\frac{P(kz/b)P(ka/w)}{P(k)P(kza/wb)}=\frac{P(ke^{-\mathrm{i}(\theta+\theta_3)})P(ke^{\mathrm{i}(-\theta+\theta_3)})}{P(k)P(ke^{-2\mathrm{i}\theta})}=\frac{P(\hat{k}e^{-\mathrm{i}\theta_3})P(\hat{k}e^{\mathrm{i}\theta_3})}{P(\hat{k}e^{-\mathrm{i}\theta})P(\hat{k}e^{\mathrm{i}\theta})}, \tag{4.5}$$

and where we have set $k=\hat{k}e^{\mathrm{i}\theta}$ because k is arbitrary. Because of this choice, $A(\theta_1,\theta,\hat{k})$ becomes independent of θ_3 and $B(\theta_3,\theta,\hat{k})$ becomes independent of θ_1.

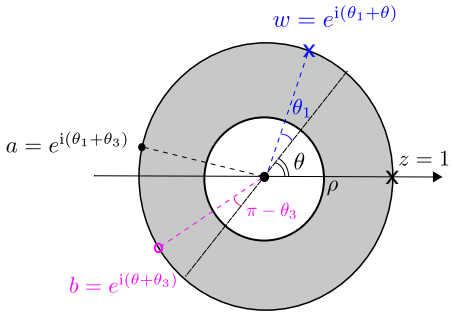

Figure 4. Special choice of angular coordinates: the angles θ_1 and θ_3 measure deviations from the symmetric choice of contact points.

The next step is to consider contour integrals of $A(\theta_1, \theta, \hat{k})$ and $B(\theta_3, \theta, \hat{k})$ with respect to $\hat{k}$ around the circle $|\hat{k}| = \rho$. From (4.3), we thus obtain an *integrated Fay trisecant identity*:

$$\alpha(\theta_1, \theta) X_{\theta_1,\theta_3,\theta} + \beta(\theta_3, \theta) Y_{\theta_1,\theta_3,\theta} = 1, \tag{4.6}$$

where

$$\alpha(\theta_1, \theta) \equiv \frac{1}{2\pi} \int_0^{2\pi} A(\theta_1, \theta, \rho e^{\mathrm{i}\phi}) d\phi = \frac{1}{2\pi} \int_0^{2\pi} \frac{P(\rho e^{\mathrm{i}(\phi-\theta_1)}) P(\rho e^{\mathrm{i}(\phi+\theta_1)})}{P(\rho e^{\mathrm{i}(\phi-\theta)}) P(\rho e^{\mathrm{i}(\phi+\theta)})} d\phi, \tag{4.7}$$

$$\beta(\theta_3, \theta) \equiv \frac{1}{2\pi} \int_0^{2\pi} B(\theta_3, \theta, \rho e^{\mathrm{i}\phi}) d\phi = \frac{1}{2\pi} \int_0^{2\pi} \frac{P(\rho e^{\mathrm{i}(\phi-\theta_3)}) P(\rho e^{\mathrm{i}(\phi+\theta_3)})}{P(\rho e^{\mathrm{i}(\phi-\theta)}) P(\rho e^{\mathrm{i}(\phi+\theta)})} d\phi. \tag{4.8}$$

The integrated Fay trisecant identity (4.6) is essential for understanding the envelope structure and proving the conjectures made about it in the literature.

On taking a derivative of (4.6) with respect to θ, we find

$$\frac{\partial \alpha(\theta_1, \theta)}{\partial \theta} X_{\theta_1,\theta_3,\theta} + \frac{\partial \beta(\theta_3, \theta)}{\partial \theta} Y_{\theta_1,\theta_3,\theta} + \alpha(\theta_1, \theta) \frac{\partial X_{\theta_1,\theta_3,\theta}}{\partial \theta} + \beta(\theta_3, \theta) \frac{\partial Y_{\theta_1,\theta_3,\theta}}{\partial \theta} = 0. \tag{4.9}$$

The sum of the first two terms is zero because

$$\frac{\partial \alpha(\theta_1, \theta)}{\partial \theta} X_{\theta_1,\theta_3,\theta} + \frac{\partial \beta(\theta_3, \theta)}{\partial \theta} Y_{\theta_1,\theta_3,\theta} \quad = \frac{\mathrm{i}}{2\pi} \int_0^{2\pi} [K(\rho e^{\mathrm{i}(\phi-\theta)}) - K(\rho e^{\mathrm{i}(\phi+\theta)})] d\phi = 0, \tag{4.10}$$

where we used the Fay identity (4.3) in the first equality. On use of (4.10) in (4.9), we find

$$\alpha(\theta_1, \theta) \frac{\partial X_{\theta_1,\theta_3,\theta}}{\partial \theta} + \beta(\theta_3, \theta) \frac{\partial Y_{\theta_1,\theta_3,\theta}}{\partial \theta} = 0. \tag{4.11}$$

Suppose now that we fix the two parameters θ_1 and θ_3. Then the points $(X_{\theta_1,\theta_3,\theta}, Y_{\theta_1,\theta_3,\theta})$ lie on some curve dependent only on the single parameter θ with the tangent at $(X_{\theta_1,\theta_3,\theta}, Y_{\theta_1,\theta_3,\theta})$, when viewed as a function of θ, defined as the set of points (X, Y) satisfying

$$Y - Y_{\theta_1,\theta_3,\theta} = \frac{\partial Y_{\theta_1,\theta_3,\theta}/\partial \theta}{\partial X_{\theta_1,\theta_3,\theta}/\partial \theta} (X - X_{\theta_1,\theta_3,\theta}). \tag{4.12}$$

If we now make use of both (4.11) and (4.6) we can see that the tangent line (4.12) is equivalent to

$$\alpha(\theta_1, \theta) X + \beta(\theta_3, \theta) Y = 1. \tag{4.13}$$

This is an important observation and it is helpful to visualize this pictorially. Figure 5 shows some examples of these tangent lines. The red line represents the collection of data points $(X_{\theta_1,\theta_3,\theta}, Y_{\theta_1,\theta_3,\theta})$ sketched out when both θ_1 and θ_3 are fixed and the parameter θ is varied; the blue lines in Figure 5, given by (4.13), are clearly tangent to those red lines (each blue line

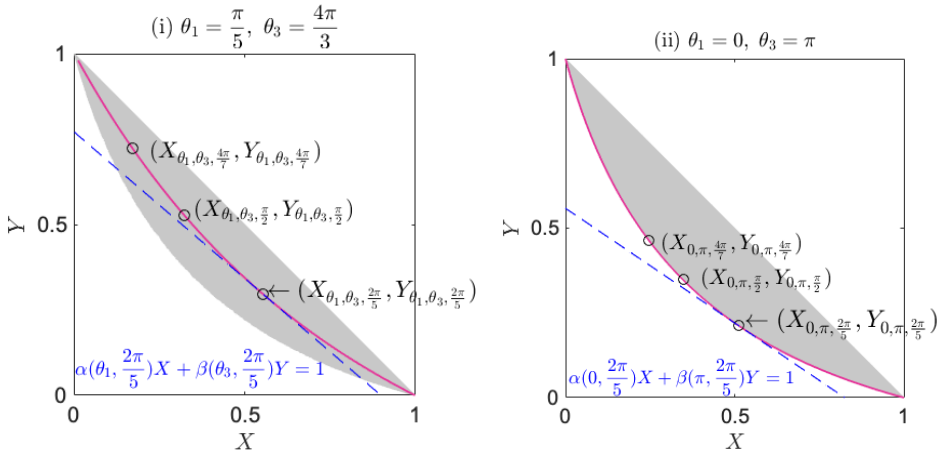

Figure 5. The red lines are collections of data points $(X_{\theta_1,\theta_3,\theta}, Y_{\theta_1,\theta_3,\theta})$ with both θ_1 and θ_3 fixed and only parameter θ changed. The blue lines, given by (4.13), are typical tangents to the red lines at $(X_{\theta_1,\theta_3,\frac{2\pi}{5}}, Y_{\theta_1,\theta_3,\frac{2\pi}{5}})$. When the fixed parameters θ_1 and θ_3 take the particular values $\theta_1 = 0$ and $\theta_3 = \pi$ the red line, parameterized by θ, corresponds to the lower envelope.

corresponds to a particular choice of θ). The important point is that, in view of the observation (4.13), and the observation made earlier that the symmetric choice of (a, b, z, w) shown in Figure 3 corresponds to $\theta_1 = 0$ and $\theta_3 = \pi$, the two inequalities in (1.12) are equivalent to

$$X + Y \le 1, \tag{4.14}$$

$$\alpha_\theta X + \beta_\theta Y \ge 1, \qquad \alpha_\theta \equiv \alpha(0,\theta), \qquad \beta_\theta \equiv \beta(\pi,\theta), \tag{4.15}$$

for all pairs (X, Y) and $0 < \theta < \pi$. The first statement simply states that all pairs (X, Y) for $\rho \ge 0$ lie on or below the line $X + Y = 1$ relevant to the classical van der Pauw case $\rho = 0$; the second statement states that all pairs (X, Y) for $\rho \ge 0$ lie above a curve, parametrized by θ associated with the symmetric choice of points shown in Figure 3, and defined for $\theta_1 = 0$ and $\theta_3 = \pi$.

The more technical details are relegated to appendix A but the overall strategy is easy to explain: we prove (4.14) and (4.15) for all (X, Y) by considering the maximum values and minimum values of the coefficient functions $\alpha(\theta_1, \theta)$ and $\beta(\theta_3, \theta)$ subject to the condition (4.2). From the integrated Fay identity (4.6) and the principles of the minimum and the maximum, we have that

$$\min_{-\theta<\theta_1<\theta}(\alpha(\theta_1,\theta))X_{\theta_1,\theta_3,\theta} + \min_{\theta<\theta_3<2\pi-\theta}(\beta(\theta_3,\theta))Y_{\theta_1,\theta_3,\theta} \le \alpha(\theta_1,\theta)X_{\theta_1,\theta_3,\theta} + \beta(\theta_3,\theta)Y_{\theta_1,\theta_3,\theta} = 1, \tag{4.16}$$

$$\max_{-\theta<\theta_1<\theta}(\alpha(\theta_1,\theta))X_{\theta_1,\theta_3,\theta} + \max_{\theta<\theta_3<2\pi-\theta}(\beta(\theta_3,\theta))Y_{\theta_1,\theta_3,\theta} \ge \alpha(\theta_1,\theta)X_{\theta_1,\theta_3,\theta} + \beta(\theta_3,\theta)Y_{\theta_1,\theta_3,\theta} = 1. \tag{4.17}$$

The strategy is illustrated schematically in Figure 6. By minimising both $\alpha(\theta_1, \theta)$ and $\beta(\theta_3, \theta)$, the upper envelope $X + Y = 1$ is obtained. In contrast, by maximising both $\alpha(\theta_1, \theta)$ and $\beta(\theta_3, \theta)$, a tangent line to the lower envelope is obtained; moreover, the explicit equation (1.13) for the curve traced out by this lower envelope arises from this analysis. Thus (4.16) is essentially equivalent to (4.14), and (4.17) is equivalent to (4.15).

While the new formula (1.13) describes the lower envelope an approximation of small $\rho \ll 1$ can be used to provide a more explicit expression of van der Pauw type relating the measured

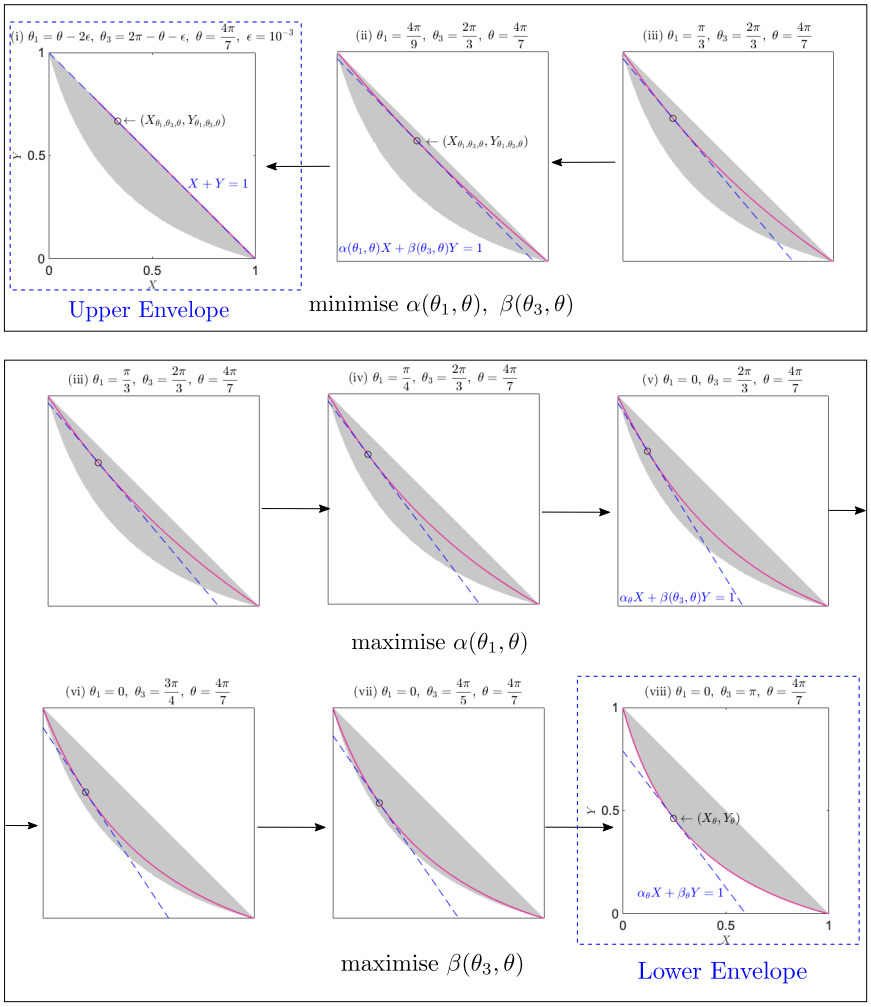

Figure 6. Visualizing the relationship between tangent lines and the upper and lower envelopes. The parameter $\theta = \frac{4\pi}{7}$ is fixed in all figures. Red lines show the curves produced by changing only θ, and blue lines are tangents to the envelope at $(X_{\theta_1,\theta_3,\theta}, Y_{\theta_1,\theta_3,\theta})$. When $\alpha(\theta_1, \theta)$ and $\beta(\theta_3, \theta)$ are minimised, the tangent line corresponds to $X + Y = 1$. When $\alpha(\theta_1, \theta)$ and $\beta(\theta_3, \theta)$ are maximised, the line becomes a tangent line to the lower envelope at (X_θ, Y_θ), where $X_\theta \equiv X_{0,\pi,\theta}$ and $Y_\theta \equiv Y_{0,\pi,\theta}$.

resistances. The values $X_{0,\pi,\theta}$ and $Y_{0,\pi,\theta}$ are

$$X_{0,\pi,\theta} = \exp\left(-\frac{R_X^\theta}{\lambda}\right) = \frac{P(-e^{\mathrm{i}\theta})P(-e^{-\mathrm{i}\theta})}{P(-1)P(-1)}, \qquad Y_{0,\pi,\theta} = \exp\left(-\frac{R_Y^\theta}{\lambda}\right) = \frac{P(e^{\mathrm{i}\theta})P(e^{-\mathrm{i}\theta})}{P(-1)P(-1)}. \tag{4.18}$$

By expanding in powers of ρ^2 and eliminating terms of order ρ^4 and higher, an approximation for the lower envelope is obtained as follows:

$$\left(\exp\left(-\frac{R_X^\theta}{\lambda}\right) + \exp\left(-\frac{R_Y^\theta}{\lambda}\right)\right)^2 + \frac{32\rho^2}{1-4\rho^2}\exp\left(-\frac{R_X^\theta + R_Y^\theta}{\lambda}\right) = 1. \tag{4.19}$$

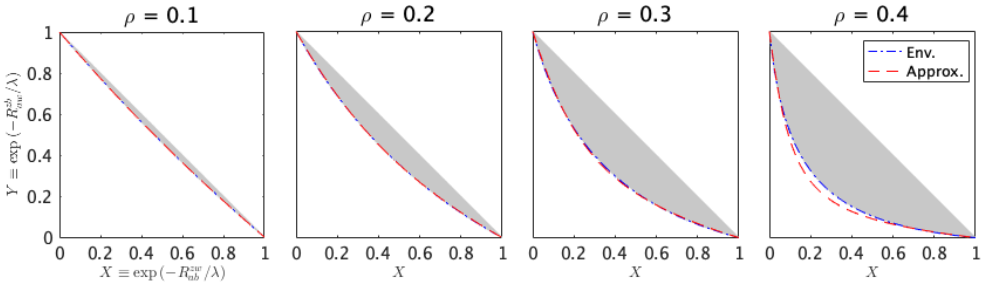

Figure 7. The approximation (4.19) of the lower envelope is superposed on data from numerical experiments for different values of ρ. The exact formula (1.13) lies precisely on the lower envelope formed by the data. For small ρ the lower envelope is well approximated by a quadratic in X and Y.

The derivation of (4.19) is given in Appendix C. Equation (4.19) includes two unknown parameters ρ and λ but ρ can be eliminated explicitly by considering the ratio of the first term and the second term in (4.19). The approximate formula (1.14) recorded earlier then follows. Roughly speaking, one would expect this formula to give good results for a sample with relatively small holes located away from the sample boundaries since then one might expect ρ to be small. In any event, (1.14) provides a useful first approximation for any sample with a single hole and will certainly be more accurate than use of (1.1). It can also provide an initial guess for an iterative solution procedure.

Figure 7 shows the comparison between the actual lower envelope (1.13) and the asymptotic expansion (4.19) as the conformal modulus ρ varies. These graphs show that the asymptotic expansion yields a very satisfactory approximation for the lower envelope when $\rho < 0.3$ and it remains quite accurate for larger ρ.

5. Determining resistivity using the lower envelope equation

A method to obtain λ based on the lower envelope has already been proposed in [12]. Because the resistance $(R^{zw}_{ab}, R^{zb}_{aw})$ from the symmetric points shown in Figure 3 can be parametrized by the angle θ the corresponding resistances can be denoted by the parameter θ as follows:

$$R^{\theta}_{X} \equiv R^{\hat{z}\hat{w}}_{\hat{a}\hat{b}}, \qquad R^{\theta}_{Y} \equiv R^{\hat{z}\hat{b}}_{\hat{a}\hat{w}}, \tag{5.1}$$

where $\hat{z} = 1 = -\hat{a}$, $\hat{w} = \exp(\mathrm{i}\theta) = -\hat{b}$, $0 < \theta < \pi$. The paper [12] proposed to measure several resistivities on the lower envelope and conducted a standard fit to obtain λ.

If the given sample has clear reflectional symmetries about two perpendicular axes, it is an easy matter to find resistances within the class (5.1) associated with symmetrically-disposed points in the preimage domain as shown in Figure 3. This is because one expects to be able to identify reflectionally symmetric points in the physical domain with reflectionally symmetric preimage points in the annulus.

However, for a generally non-symmetric sample it is not obvious how one might obtain this resistance information for such symmetrically-disposed points in the preimage domain. If one knows the conformal mapping to the given doubly connected sample from a preimage annulus then the contact points corresponding to such symmetric preimage points can be determined in principle. However, one of the advantages of the traditional van der Pauw method is that it exploits the underlying conformal invariance of the problem; this manifests itself in a practical way by formula (1.1) being valid for *any* shapes and, in particular, without the need to determine any conformal mapping functions. Ideally, any practical method for a holey sample should also avoid the need to compute any conformal mappings.

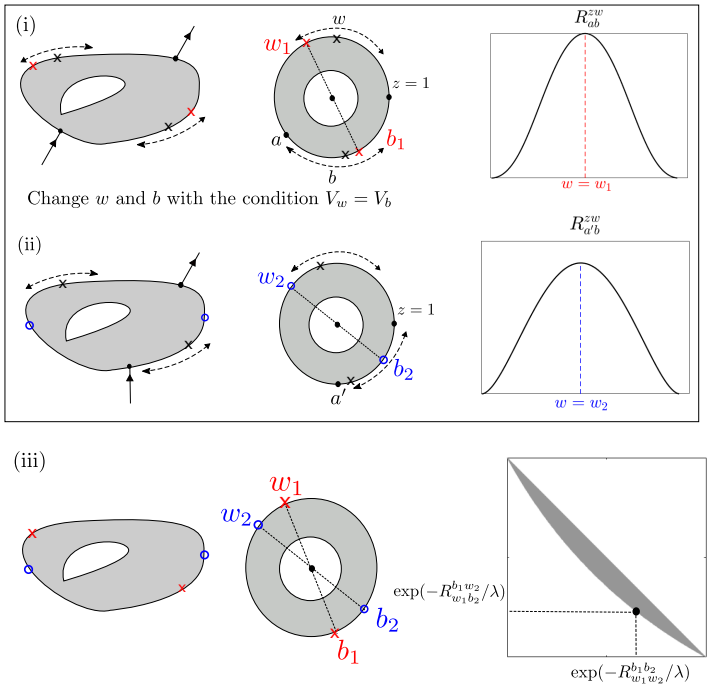

Figure 8. (i), (ii) Illustration of the practical procedure, proposed in [12], to obtain contact points w_1, b_1, w_2, b_2 with the symmetry shown in Figure 3. By searching for the local extrema of R^{zw}_{ab} a symmetrical choice of points shown in (iii), and corresponding to resistances lying on the lower envelope, can be found.

A practical method has been proposed in [12] based on searching for the extrema of the resistance measurements. That procedure is as follows: firstly, as shown in (i) in Figure 8, arbitrary points are chosen on the sample boundary with preimage points z and a with a source placed at z and a sink at a. Then, by changing the two contact points with preimages w and b, with the condition that the potential at w remains the same as the potential at b, the local extremum of the measured resistance R^{zw}_{ab} is found. When the resistance R^{zw}_{ab} is at the local extremum, the claim in [12] is that the line wb become diametrically opposed points in the preimage annulus; this special choice of points are then marked as w_1 and b_1. In a second step, as shown in (ii) in Figure 8, the point a is changed to a', and the same procedure as in (i) is repeated in order to obtain a second such diametrically-opposed pair w_2 and b_2. It is then clear from (iii) in Figure 8 that the four-point pair (w_1, w_2, b_1, b_2) has the sought-after symmetry shown in Figure 3 and which, therefore, correspond to resistance measurements that lie on the lower envelope.

Szymański et al. [12] verified experimentally that this method works, but appeared not to give any mathematical explanation of *why* it works. We now provide such an explanation.

When there are a source a and sink z as shown in (i) in Figure 8, the potential difference between w and b is

$$V_{wb} \equiv V_w - V_b = \lambda J_{az} \log \frac{P(w/a)P(b/z)}{P(w/z)P(b/a)}. \tag{5.2}$$

Suppose we search for a local extremum of R^{zw}_{ab} while changing w and b with the condition that $V_{wb} = 0$. This problem is expressed mathematically using a Lagrange multiplier γ:

$$F(w,b) \equiv \frac{1}{\lambda}(R^{zw}_{ab} + \gamma V_{wb}) = \log \frac{P(z/a)P(w/b)}{P(z/b)P(w/a)} + \hat{\gamma} \log \frac{P(w/a)P(b/z)}{P(w/z)P(b/a)}, \tag{5.3}$$

where $\hat{\gamma} \equiv \gamma / J_{az}$. By considering the derivative with respect to w and b, we obtain two conditions for local extrema:

$$\frac{\partial F}{\partial w} = \frac{1}{w}[K(w/b) - K(w/a)) + \hat{\gamma}(K(w/a) - K(w/z))] = 0, \tag{5.4}$$

$$\frac{\partial F}{\partial b} = \frac{1}{b}[K(z/b) - K(w/b)) + \hat{\gamma}(K(b/z) - K(b/a))] = 0. \tag{5.5}$$

It can be verified that both conditions are satisfied when $w = -b$ and $a/w = w/z$, which correspond to the symmetric choice of contact points. This explains why the practical procedure just described does indeed pick out points with diametrically-opposed preimages w and b in the annulus.

In view of the above discussion we now proceed under the assumption that two pairs of resistances $(R_X^{\theta_j}, R_Y^{\theta_j})$, $j = 1,\ 2$, for two sets of contact points in the symmetric arrangement shown in Figure 3 are available. The method proposed here is to make use of the two explicit formulas (1.13) and (1.14) to determine λ.

Some simple numerical experiments validate that λ can indeed be robustly found using the new expressions (1.13) and (1.14) for the lower envelope. We set $\lambda = 0.25$ and then used the explicit formulas for the voltage based on (2.8) to generate the "data" giving the resistances corresponding to two four-point pairs in symmetric configurations around C_0; in a real experiment, this data would be found by measurement on the physical sample such as those just described. Those values are used both in (two instances of) formula (1.13) and in the single approximate formula (1.14) and a standard nonlinear solver (interior-point method) is used to solve them for λ. Table 1 show the values of λ and ρ. As expected, the methods retrieve the known results to the expected degrees of accuracy.

Table 1. Numerical determination of λ and ρ on solving (1.13) and (1.14)

λ	(i)	(ii)	(iii)
Env. method	0.25000	0.25000	0.25000
Approx. method	0.25061	0.25705	0.27608
True value	0.25	0.25	0.25
ρ	(i)	(ii)	(iii)
Env. method	0.100001	0.20000	0.30000
Approx. method	0.097726	0.18445	0.25401
True value	0.1	0.2	0.3

6. Discussion

This paper has demonstrated the importance of the prime function associated with a concentric annulus, and the Fay trisecant identity expressible in terms of it, to extending the well-known van der Pauw method to measuring the resistivity of a sample with a hole.

By considering an integrated form of the Fay trisecant identity, we have derived an explicit formula (1.13) for the lower envelope formed by the resistance measurements from sets of symmetrically-disposed contact points shown in Figure 3. An approximate form (1.14) more closely resembling the original van der Pauw formula (1.1) has also been given depending on 4 symmetric resistance measurements instead of 2.

Using these same mathematical tools, we have also been able to justify mathematically a number of conjectures made in the literature. Those results have been described here with full technical details available in [25].

The van der Pauw method for a sample with two or more holes is, of course, of interest and several studies have recently appeared [13,15]. The significance of the mathematical tools we have

introduced here to the van der Pauw problem is that they all have natural higher-genus analogues, that is, natural extensions to domains of higher connectivity. The monograph [9] is dedicated to the theory of the prime function on planar domains of general finite connectivity, and the relevance of the prime function to expressing the complex potential for source/sink flows in such domains is already known [26]. At the same time, the Fay trisecant identity also carries over to higher genus Riemann surfaces [23,24]. Therefore, while we have focused here on what we believe to be the simplest non-trivial case of a holey sample, we expect all the ideas to be extendible to the case of a sample with any finite number of holes.

Data Accessibility. This article has no additional data.

Authors' Contributions. All authors contributed to the contents of this paper during the course of the first author's PhD project under the supervision of the second author.

Competing Interests. We declare we have no competing interests.

Funding. The Nakajima Foundation.

Acknowledgements. H.M. is grateful to The Nakajima Foundation in Japan for financial support. All authors acknowledge support from EPSRC grant EP/R014604/1 during the "Complex analysis: techniques, applications and computations" programme at the Newton Institute in Cambridge (Sep.–Dec. 2019).

A. Analysis of the upper and lower envelopes

To study the extrema of $\alpha(\theta_1,\theta)$ and $\beta(\theta_1,\theta)$ in (4.16) and (4.17) we define an important function

$$g_\theta(\eta) \equiv \frac{1}{2\pi}\int_0^{2\pi} \frac{P(\rho e^{\mathrm{i}(\phi-\eta)})P(\rho e^{\mathrm{i}(\phi+\eta)})}{P(\rho e^{\mathrm{i}(\phi-\theta)})P(\rho e^{\mathrm{i}(\phi+\theta)})}\,d\phi, \tag{A.1}$$

where $0 \le \eta \le 2\pi$. This function is significant because, from (4.8) it is clear that the two coefficients functions in (4.6) can be written

$$\alpha(\theta_1,\theta) = g_\theta(\theta_1), \qquad \beta(\theta_3,\theta) = g_\theta(\theta_3). \tag{A.2}$$

Analysis of this function $g_\theta(\eta)$ provides the key to justifying the conjectures. The function arises naturally from the integrated Fay trisecant identity.

Figure 9 shows the typical behaviour of the function $g_\theta(\eta)$ for a range of ρ values; recall that the function $P(\zeta)$, and hence $g_\theta(\eta)$, depends on the parameter ρ. A companion paper [25] provides details showing that $g_\theta(\eta)$ has this same qualitative form for all admissible ρ.

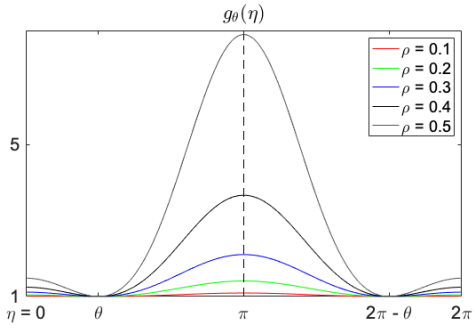

Figure 9. Behavior of the function $g_\theta(\eta)$. A local maximum of $g_\theta(\eta)$ is obtained when $\eta = 0$ or $\eta = \pi$. A local minimum of $g_\theta(\eta)$ is obtained when $\eta = \theta$ or $2\pi - \theta$. It can be proven [25] that $g_\theta(\eta)$ has this qualitative structure for any $0 < \rho < 1$.

Upper envelope: Figure 9 suggests that, for any value $0 < \rho < 1$, $g_\theta(\eta)$ attains a local minimum when $\eta = \theta, 2\pi - \theta$. Moreover it is clear that, at these local minima, the extremal values of $\alpha(\theta_1,\theta)$

and $\beta(\theta_3,\theta)$ is 1. This fact, combined with (4.16) and (A.2), imply that

$$X_{\theta_1,\theta_3,\theta} + Y_{\theta_1,\theta_3,\theta} \leq 1 \tag{A.3}$$

for all $(X_{\theta_1,\theta_3,\theta}, Y_{\theta_1,\theta_3,\theta})$. This defines the upper envelope (4.14).

Lower envelope: Figure 9 also suggests that, for any value $0<\rho<1$, $g_\theta(\eta)$ attains a local maximum when $\eta=0,\pi$. On use of (A.2) the maxima of $\alpha(\theta_1,\theta)$ and $\beta(\theta_3,\theta)$ occur when $\theta_1=0$ and $\theta_3=\pi$. Hence, from (4.17) and (A.2) we conclude that

$$\alpha_\theta X_{\theta_1,\theta_3,\theta} + \beta_\theta Y_{\theta_1,\theta_3,\theta} \geq 1, \qquad \alpha_\theta \equiv \alpha(0,\theta), \qquad \beta_\theta \equiv \beta(\pi,\theta). \tag{A.4}$$

This shows that the pair of measurements $(X_{\theta_1,\theta_3,\theta}, Y_{\theta_1,\theta_3,\theta})$ lies above the tangent line at $(X_{0,\pi,\theta}, Y_{0,\pi,\theta})$. Note that this result holds under the assumption that θ is fixed. The final step, in order to prove that this set of tangent lines forms a lower envelope for the resistance measurements, is to show that for any other choice $\theta'\neq\theta$, the pair of measurements $(X_{\theta_1,\theta_3,\theta}, Y_{\theta_1,\theta_3,\theta})$ *also* lies above the tangent line at $(X_{0,\pi,\theta'}, Y_{0,\pi,\theta'})$. This is equivalent to showing that

$$\alpha_{\theta'} X_{\theta_1,\theta_3,\theta} + \beta_{\theta'} Y_{\theta_1,\theta_3,\theta} \geq 1. \tag{A.5}$$

To show (A.5), we note first from the definition of $P(\zeta)$ in (2.4),

$$P(\rho e^{\mathrm{i}\phi}) = \prod_{n=1}^{\infty} (1+\rho^{4n-2} - 2\rho^{2n-1}\cos\phi) > 0, \tag{A.6}$$

which means both $A(\theta_1,\theta_3,\rho e^{\mathrm{i}\phi})$ and $B(\theta_1,\theta_3,\rho e^{\mathrm{i}\phi})$ are real and positive. We can therefore use a sum-log and log-sum inequality in the integral as follows:

$$\begin{aligned}
&\log\left[\alpha_{\theta'} X_{\theta_1,\theta_3,\theta} + \beta_{\theta'} Y_{\theta_1,\theta_3,\theta}\right] \\
&\quad\geq \log\left[\alpha(\theta_1,\theta') X_{\theta_1,\theta_3,\theta} + \beta(\theta_3,\theta') Y_{\theta_1,\theta_3,\theta}\right] \\
&\quad= \log\left[\frac{1}{2\pi}\int_0^{2\pi} (A(\theta_1,\theta',\rho e^{\mathrm{i}\phi}) X_{\theta_1,\theta_3,\theta} + B(\theta_3,\theta',\rho e^{\mathrm{i}\phi}) Y_{\theta_1,\theta_3,\theta}) d\phi\right] \\
&\quad\geq \frac{1}{2\pi}\int_0^{2\pi} \log\left[A(\theta_1,\theta',\rho e^{\mathrm{i}\phi}) X_{\theta_1,\theta_3,\theta} + B(\theta_3,\theta',\rho e^{\mathrm{i}\phi}) Y_{\theta_1,\theta_3,\theta}\right] d\phi.
\end{aligned} \tag{A.7}$$

Now the right hand side of this inequality can be written as

$$\begin{aligned}
&\frac{1}{2\pi}\int_0^{2\pi} \log\left[X_{\theta_1,\theta_3,\theta} + \frac{B(\theta_3,\theta',\rho e^{\mathrm{i}\phi})}{A(\theta_1,\theta',\rho e^{\mathrm{i}\phi})} Y_{\theta_1,\theta_3,\theta}\right] d\phi + \frac{1}{2\pi}\int_0^{2\pi} \log A(\theta_1,\theta',\rho e^{\mathrm{i}\phi}) d\phi \\
&= \frac{1}{2\pi}\int_0^{2\pi} \log\left[X_{\theta_1,\theta_3,\theta} + \frac{B(\theta_3,\theta,\rho e^{\mathrm{i}\phi})}{A(\theta_1,\theta,\rho e^{\mathrm{i}\phi})} Y_{\theta_1,\theta_3,\theta}\right] d\phi + \frac{1}{2\pi}\int_0^{2\pi} \log A(\theta_1,\theta,\rho e^{\mathrm{i}\phi}) d\phi \\
&= \frac{1}{2\pi}\int_0^{2\pi} \log\left[A(\theta_1,\theta,\rho e^{\mathrm{i}\phi}) X_{\theta_1,\theta_3,\theta} + B(\theta_3,\theta,\rho e^{\mathrm{i}\phi}) Y_{\theta_1,\theta_3,\theta}\right] d\phi = 0,
\end{aligned} \tag{A.8}$$

where we used the fact that the integral of $\log A(\theta_1,\theta,\rho e^{\mathrm{i}\phi})$ is zero and the fact that

$$\frac{B(\theta_1,\theta',\rho e^{\mathrm{i}\phi})}{A(\theta_3,\theta',\rho e^{\mathrm{i}\phi})} = \frac{B(\theta_1,\theta,\rho e^{\mathrm{i}\phi})}{A(\theta_3,\theta,\rho e^{\mathrm{i}\phi})} = \frac{P(\rho e^{\mathrm{i}(\phi-\theta_3)}) P(\rho e^{\mathrm{i}(\phi+\theta_3)})}{P(\rho e^{\mathrm{i}(\phi-\theta_1)}) P(\rho e^{\mathrm{i}(\phi+\theta_1)})}, \tag{A.9}$$

so that this ratio is independent of the middle argument of the numerator and denominator (that is, either θ or θ' in (A.9)). See Appendix B for the integral of $\log A(\theta_1,\theta,\rho e^{\mathrm{i}\phi})$. Putting all these pieces together we have shown that

$$\log\left[\alpha_{\theta'} X_{\theta_1,\theta_3,\theta} + \beta_{\theta'} Y_{\theta_1,\theta_3,\theta}\right] \geq 0 \tag{A.10}$$

which is equivalent, on exponentiation, to (A.5). Each step in the proof is shown schematically in Figure 10.

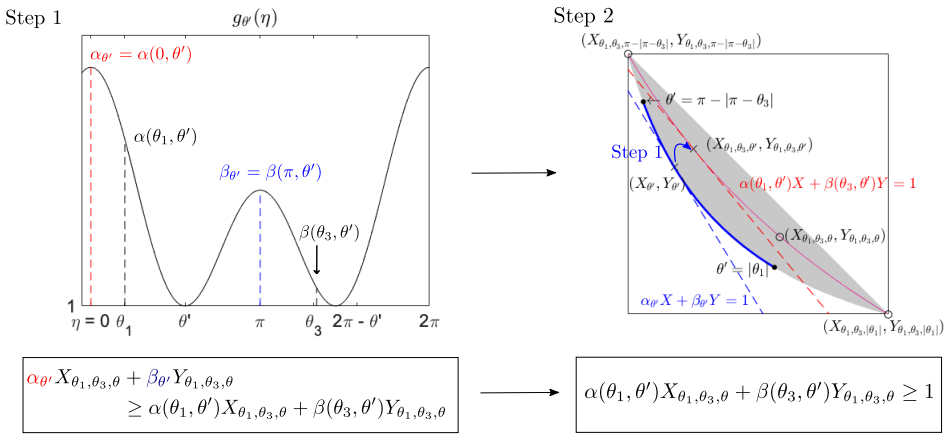

Figure 10. Schematic illustrating the idea of the proof that $\alpha_{\theta'} X_{\theta_1,\theta_3,\theta} + \beta_{\theta'} Y_{\theta_1,\theta_3,\theta} \geq 1$ for any $0 < \theta' < \pi$. For simplicity, we focus on the case such that $\alpha_{\theta'} \geq \alpha(\theta_1,\theta')$ and $\beta_{\theta'} \geq \beta(\theta_3,\theta')$. After Step 1, a sum-log and log-sum inequality is used to prove that $\alpha(\theta_1,\theta')X_{\theta_1,\theta_3,\theta} + \beta(\theta_3,\theta')Y_{\theta_1,\theta_3,\theta} \geq 1$ in Step 2. Once this is done for every point on the lower envelope (i.e., for any $0 < \theta' < \pi$ and there are three cases to consider) we establish that the point $(X_{\theta_1,\theta_3,\theta}, Y_{\theta_1,\theta_3,\theta})$ is to the right of the lower envelope.

For simplicity in this exposition, we focus on the case that $\alpha_{\theta'} \geq \alpha(\theta_1,\theta')$ and $\beta_{\theta'} \geq \beta(\theta_3,\theta')$ which is illustrated in Figure 10. This case corresponds to the particular choice of $(\theta_1,\theta_3,\theta')$ such that $|\theta_1| \leq \theta' \leq \pi - |\pi - \theta_3|$ as shown in the blue line in Figure 10. Thus, there are two other cases to be considered: $0 < \theta' < |\theta_1|$ and $\pi - |\pi - \theta_3| < \theta' < \pi$. An outline of the technical arguments will be summarized here. When $\theta' < |\theta_1|$, it can be shown that $\alpha_{\theta'} \geq \alpha(\theta_1, |\theta_1|)$ and $\beta_{\theta'} \geq \beta(\theta_3, |\theta_1|)$. When $\pi - |\pi - \theta_3| < \theta'$, it can be shown that $\alpha_{\theta'} \geq \alpha(\theta_1, \pi - |\pi - \theta_3|)$ and $\beta_{\theta'} \geq \beta(\theta_3, \pi - |\pi - \theta_3|)$. In any of these cases, we can use the same technique (a log-sum and sum-log inequality) to prove (A.5). It is clear that the features of the function $g_\theta(\eta)$ evident from Figure 9 are the crucial facts needed to establish the envelope structure. It is necessary to prove that the function $g_\theta(\eta)$ always behaves in this way for any value of ρ. Full technical details can be found in [25].

We conclude that for $0 < \theta < \pi$ and for all (X,Y), $\alpha_\theta X + \beta_\theta Y \geq 1$ for all (X,Y). In this way, we have identified the lower envelope.

The formula (1.13) for the lower envelope follows from (A.8) on setting $\theta_1 = 0, \theta_3 = \pi$:

$$\frac{1}{2\pi}\int_0^{2\pi} \log\left[X_{0,\pi,\theta} + \frac{B(\pi,\theta,\rho e^{\mathrm{i}\phi})}{A(0,\theta,\rho e^{\mathrm{i}\phi})} Y_{0,\pi,\theta}\right] d\phi = 0. \tag{A.11}$$

Using the definitions in (4.4)–(4.5), and with $X_{0,\pi,\theta} = \exp(-R_X^\theta/\lambda)$, and $Y_{0,\pi,\theta} = \exp(-R_Y^\theta/\lambda)$, we obtain (1.13).

B. The integral of $\log A(\theta_1, \theta, \rho e^{\mathrm{i}\phi})$

This result follows from the observation

$$\frac{1}{2\pi}\int_0^{2\pi} \log A(\theta_1,\theta,\rho e^{\mathrm{i}\phi}) d\phi = \frac{1}{2\pi}\int_0^{2\pi} \log\left(\frac{P(\rho e^{\mathrm{i}(\phi-\theta_1)})P(\rho e^{\mathrm{i}(\phi+\theta_1)})}{P(\rho e^{\mathrm{i}(\phi-\theta)})P(\rho e^{\mathrm{i}(\phi+\theta)})}\right) d\phi$$

$$= \frac{1}{2\pi}\int_0^{2\pi} [\log P(\rho e^{\mathrm{i}(\phi-\theta_1)}) + \log P(\rho e^{\mathrm{i}(\phi+\theta_1)}) - \log P(\rho e^{\mathrm{i}(\phi-\theta)}) - \log P(\rho e^{\mathrm{i}(\phi+\theta)})] d\phi = 0. \tag{B.1}$$

C. Deviation of (4.19)

Here we derive a formula for the lower envelope under the assumption that $\rho \ll 1$. From the definitions of $X_{0,\pi,\theta}$ and $Y_{0,\pi,\theta}$ it follows that

$$X_{0,\pi,\theta} = \frac{P(-e^{\mathrm{i}\theta})P(-e^{-\mathrm{i}\theta})}{P(-1)P(-1)} \sim \frac{(1+\cos\theta)(1+4\rho^2\cos\theta)}{2(1+4\rho^2)}, \tag{C.1}$$

$$Y_{0,\pi,\theta} = \frac{P(e^{\mathrm{i}\theta})P(e^{-\mathrm{i}\theta})}{P(-1)P(-1)} \sim \frac{(1-\cos\theta)(1-4\rho^2\cos\theta)}{2(1+4\rho^2)}, \tag{C.2}$$

where we used the first order approximation in ρ^2:

$$P(\zeta) \sim (1-\zeta)(1-\rho^2\zeta)(1-\rho^2\zeta^{-1}) + \mathcal{O}(\rho^4). \tag{C.3}$$

We can calculate

$$(1-4\rho^2)(X_{0,\pi,\theta}+Y_{0,\pi,\theta})^2 + 32\rho^2 X_{0,\pi,\theta}Y_{0,\pi,\theta} = \frac{(1-4\rho^2)(1+4\rho^2\cos^2\theta)^2 + 8\rho^2\sin^2\theta}{(1+4\rho^2)^2}$$
$$= \frac{1}{1+4\rho^2} + \mathcal{O}(\rho^4) = 1 - 4\rho^2 + \mathcal{O}(\rho^4).$$

Since $X_{0,\pi,\theta} = \exp(-R_X^\theta/\lambda)$ and $Y_{0,\pi,\theta} = \exp(-R_Y^\theta/\lambda)$, we obtain

$$\left(\exp\left(-\frac{R_X^\theta}{\lambda}\right) + \exp\left(-\frac{R_Y^\theta}{\lambda}\right)\right)^2 + \frac{32\rho^2}{1-4\rho^2}\exp\left(-\frac{R_X^\theta + R_Y^\theta}{\lambda}\right) = 1. \tag{C.4}$$

References

1. Singh Y. 2013 Electrical resistivity measurements: a review. In *Int. J. Mod. Phys. Conf. Ser.* **22**, 745–756. World Scientific.
2. Miccoli I, Edler F, Pfnür H, Tegenkamp C. 2015 The 100th anniversary of the four-point probe technique: the role of probe geometries in isotropic and anisotropic systems. *J. Phys. Condens. Matter* **27**, 223201.
3. Pauw LJVD. 1958a A method of measuring the resistivity and Hall coefficient on lamellae of arbitrary shape. *Philips Tech. Rev.* **20**, 220–224.
4. Pauw LJVD. 1958b A method of measuring specific resistivity and Hall effect of discs of arbitrary shape. *Philips Res. Rep.* **13**, 1–9.
5. Wick RF. 1954 Solution of the field problem of the germanium gyrator. *J. Appl. Phys.* **25**, 741.
6. Abanin DA, Levitov L. 2008 Conformal invariance and shape-dependent conductance of graphene samples. *Phys. Rev. B* **78**, 035416.
7. Sun Y, Shi J, Meng Q. 1996 Measurement of sheet resistance of cross microareas using a modified van der Pauw method. *Semicon. Sci. Tech.* **11**, 805.
8. Cieśliński JL. 2012 Modified van der Pauw method based on formulas solvable by the Banach fixed point method. *Thin Solid Films* **522**, 314–317.
9. Crowdy D. 2020 *Solving Problems in Multiply Connected Domains.* CBMS-NSF Regional Conf. Ser. in Appl. Math. SIAM.
10. Ablowitz MJ, Fokas AS, Fokas A. 2003 *Complex variables: introduction and applications.* Cambridge University Press.
11. Szymański K, Cieśliński JL, Łapiński K. 2013 Van der Pauw method on a sample with an isolated hole. *Phys. Lett. A* **377**, 651–654.
12. Szymański K, Łapiński K, Cieśliński JL. 2015 Determination of the Riemann modulus and sheet resistance of a sample with a hole by the van der Pauw method. *Meas. Sci. Technol.* **26**, 055003.
13. Oh D, Ahn C, Kim M, Park EK, Kim YS. 2016 Application of the van der Pauw method for samples with holes. *Meas. Sci. Technol.* **27,** 12.
14. Sun ZH, Zhou J, Xia XJ, Zhou DM. 2017 Two-dimensional electrostatic model for the Van der Pauw method. *Phys. Lett. A* **381**, 2144–2148.

15. Szymański K, Walczyk C, Cieśliński JL. 2019 Determination of topological properties of thin samples by the van der Pauw method. *Measurement* **145**, 568–572.
16. Szymański K, Łapiński K, Cieśliński JL, Kobus A, Zaleski P, Biernacka M, Perzyńska K. 2015 Determination of the Riemann modulus and sheet resistivity by a six-point generalization of the van der Pauw method. *Meas. Sci. Technol.* **26**, 1–9.
17. Szymański K, Zaleski P. 2017 Precise Measurement of Inhomogeneity of 2-D System by Six-Point Method. *IEEE Trans. Instrum. Meas.* **66** 1243–1247.
18. Koon D, Wang F, Petersen D, Hansen O. 2014 Sensitivity of resistive and Hall measurements to local inhomogeneities: Finite-field, intensity, and area corrections. *J. Appl. Phys.* **116**, 133706, AIP Publishing LLC.
19. Koon D, Heřmanová M, Náhlík J. 2015 Electrical conductance sensitivity functions for square and circular cloverleaf van der Pauw geometries. *Meas Sci Technol.* **26**, 115004.
20. Ausserlechner U. 2019 The Classical Hall Effect in Multiply-Connected Plane Regions Part I:Topologies with Stream Function. *J. Appl. Math. Phys.* **7**, 1968–1996.
21. Náhlík J, Kaŝpárková I, Fitl P. 2011 Study of quantitative influence of sample defects on measurements of resistivity of thin films using van der Pauw method. *Measurement* **44**, 1968–1979.
22. Nehari Z. 2012 *Conformal mapping.* Courier Corporation.
23. Fay JD. 2006 *Theta functions on Riemann surfaces* **352**. Springer.
24. Poor C. 1992 Fay's trisecant formula and cross-ratios. *Proc. Amer. Math. Soc.* **114**, 667–671
25. Miyoshi H, Crowdy D, Nelson R. 2020 The Fay trisecant identity and the van der Pauw method. *Comput. Methods Funct. Theory (submitted).*
26. Crowdy D. 2013 Analytical formulae for source and sink flows in multiply connected domains. *Theor. Comp. Fluid Dyn.* **27**, 1–19.